

Elastic scattering for the ^8B and $^7\text{Be} + ^{208}\text{Pb}$ systems at near-Coulomb barrier energies

M. Mazzocco^{1,2,*}, N. Keeley,³ A. Boiano,⁴ C. Boiano,⁵ M. La Commara,^{6,4} C. Manea,^{2,†} C. Parascandolo,⁴ D. Pierroutsakou,⁴ C. Signorini,^{1,2} E. Strano,^{1,2} D. Torresi,^{1,2,‡} H. Yamaguchi,⁷ D. Kahl,^{7,§} L. Acosta,^{8,9,||} P. Di Meo,⁴ J. P. Fernandez-Garcia,^{9,¶} T. Glodariu,^{10,#} J. Grebosz,¹¹ A. Guglielmetti,^{12,5} Y. Hirayama,¹³ N. Imai,^{7,13} H. Ishiyama,¹³ N. Iwasa,¹⁴ S. C. Jeong,^{13,15} H. M. Jia,¹⁶ Y. H. Kim,¹³ S. Kimura,^{13,**} S. Kubono,^{7,17} G. La Rana,^{18,4} C. J. Lin,¹⁶ P. Lotti,² G. Marquínez-Durán,⁸ I. Martel,^{8,19} H. Miyatake,¹³ M. Mukai,¹³ T. Nakao,⁷ M. Nicoletto,² A. Pakou,²⁰ K. Rusek,²¹ Y. Sakaguchi,⁷ A. M. Sánchez-Benítez,^{22,23} T. Sava,¹⁰ O. Sgouros,^{20,‡} V. Soukeras,^{20,‡} F. Soramel,^{1,2} E. Stiliaris,²⁴ L. Stroe,¹⁰ T. Teranishi,²⁵ N. Toniolo,²⁶ Y. Wakabayashi,¹⁷ Y. X. Watanabe,¹³ L. Yang,^{16,7} Y. Y. Yang,²⁷ and H. Q. Zhang¹⁶

¹Dipartimento di Fisica e Astronomia, Università di Padova, via F. Marzolo 8, I-35131 Padova, Italy

²INFN-Sezione di Padova, via F. Marzolo 8, I-35131 Padova, Italy

³National Centre for Nuclear Research, ul. Andrzeja Sołtana 7, 05-400 Otwock, Poland

⁴INFN-Sezione di Napoli, via Cintia, I-80126 Napoli, Italy

⁵INFN-Sezione di Milano, via Celoria 16, I-20133 Milano, Italy

⁶Dipartimento di Farmacia, Università di Napoli “Federico II”, via D. Montesano, I-80131 Napoli, Italy

⁷Center for Nuclear Study (CNS), The University of Tokyo, Wako Branch, 2-1 Hirosawa, Wako, Saitama 351-0198, Japan

⁸Departamento de Física Aplicada, Universidad de Huelva, Campus de El Carmen, E-21071 Huelva, Spain

⁹INFN-Sezione di Catania, via Santa Sofia 64, I-95123 Catania, Italy

¹⁰NIPNE, 30 Reactorului Street, 077125 Magurele, Romania

¹¹Institute of Nuclear Physics Polish Academy of Science, ul. Radzikowskiego 152, 31-342 Kraków, Poland

¹²Università degli Studi di Milano, Dipartimento di Fisica, Via Celoria 16, I-20133 Milano, Italy

¹³KEK, Oho 1-1, Tsukuba, Ibaraki 305-0801, Japan

¹⁴Department of Physics, Tohoku University, Sendai, Miyagi 980-8578, Japan

¹⁵Institute for Basic Science (IBS), 55, Expo-ro, Yuseong-gu, 34126 Daejeon, Korea

¹⁶China Institute of Atomic Energy, P.O. Box 275, Beijing 102413, China

¹⁷RIKEN, 2-1 Hirosawa, Wako, Saitama 351-0198, Japan

¹⁸Dipartimento di Fisica, Università di Napoli “Federico II”, via Cintia, I-80126 Napoli, Italy

¹⁹Department of Physics, University of Liverpool, Liverpool L69 7ZE, United Kingdom

²⁰Department of Physics and HINP, University of Ioannina, 45110 Ioannina, Greece

²¹Heavy Ion Laboratory, University of Warsaw, ul. Pasteura 5a, 02-093 Warsaw, Poland

²²Nuclear Physics Center, University of Lisbon, P-1649-003 Lisbon, Portugal

²³Centro de Estudios Avanzados en Física, Matemáticas y Computación (CEAFMC), Department of Integrated Sciences, University of Huelva, E-21071 Huelva, Spain

²⁴Institute of Accelerating Systems and Applications and Department of Physics, University of Athens, Athens, Greece

²⁵Department of Physics, Kyushu University, Motoooka 744, Fukuoka 819-0395, Japan

²⁶INFN-LNL, viale dell'Università 2, I-35020 Legnaro (PD), Italy

²⁷Institute of Modern Physics, Chinese Academy of Sciences, 509 Nanchang Road, Lanzhou 730000, China



(Received 7 June 2019; published 1 August 2019)

The elastic scattering of the weakly bound radioactive nuclei ^8B and ^7Be from a ^{208}Pb target was measured for the first time in the energy range around the Coulomb barrier. The data were analyzed using the optical model and the continuum discretized coupled channels (CDCC) formalisms. The reaction cross sections extracted from the optical model fits clearly indicate a remarkably enhanced reaction probability for the very weakly bound ^8B ($S_p = 137.5$ keV) compared to similar mass nuclei interacting with the same target nucleus. CDCC calculations assuming a $^3\text{He} + ^4\text{He}$ cluster model well described the ^7Be experimental elastic scattering angular distributions, whereas the use of a $^7\text{Be} + p$ cluster model of ^8B with an inert ^7Be core gave a relatively poor description of the corresponding experimental data, suggesting that this model may be too simplistic and the possibility of core excitation should not be ignored.

DOI: [10.1103/PhysRevC.100.024602](https://doi.org/10.1103/PhysRevC.100.024602)

*marco.mazzocco@pd.infn.it

†Present address: INFN-TIFPA, Via Sommarive 14, I-38123 Povo (TN), Italy.

‡Present address: INFN-Laboratori Nazionali del Sud (LNS), via Santa Sofia 62, I-95123 Catania, Italy.

I. INTRODUCTION

The investigation of the reaction dynamics of light weakly bound nuclei in the energy range around the Coulomb barrier has attracted the interest of the low-energy nuclear physics community for many years now. Several review articles have been published on this subject, e.g., Refs. [1–9]. Light weakly bound nuclei are characterized by very low nucleon separation energies, typically one order of magnitude smaller than for stable nuclei located along the valley of β stability, and, in most cases, by well pronounced cluster structures. These features can generate nuclei with exotic shapes, such as the “halo” nuclei, which may be described as a well-bound inert core surrounded by a halo of rarefied nuclear matter. Depending on the type and the number of nucleons in the nuclear halo, we may have $1n$ -halo nuclei like ^{11}Be ($S_n = 0.501$ MeV), $2n$ -halo nuclei such as ^6He ($S_{2n} = 0.972$ MeV) and ^{11}Li ($S_{2n} = 0.369$ MeV), or possible $1p$ -halo nuclei, for instance the proton-halo candidate ^8B ($S_p = 0.1375$ MeV).

The low binding energy and the presence of the nuclear halo contribute to enlarging the variety of nuclear reaction mechanisms which can be triggered by these exotic projectiles. The situation is particularly remarkable in the energy range around the Coulomb barrier, where several reaction channels open up. Being very weakly bound, the projectile can more easily break up while in the proximity of the target Coulomb and nuclear fields, or one of its constituent clusters may be readily transferred or fuse with the target. All these processes are strongly interconnected to each other. Depending on how the breakup channel was modeled, either enhancement or hindrance of the sub-barrier fusion cross section was predicted. Despite earlier measurements [10,11], it was soon realized that breakup related effects increase the total reaction cross section rather than the fusion probability (Ref. [1] and references therein) and that the enhanced reactivity of weakly bound nuclei was essentially due to direct processes, especially at sub-barrier energies.

The investigation then moved to understanding what direct processes were mostly responsible for the observed enhancement of the reaction cross section. A series of measurements performed with the $2n$ -halo nucleus ^6He [12–21], the neutron skin nucleus ^8He [22–25], and ^8Li [26,27] indicated neutron transfer channels as the most dominant reaction mechanisms at near-barrier energies. More recently, experiments performed with the $2n$ -halo ^{11}Li [28,29] and the $1n$ -halo ^{11}Be

[30,31] also pointed out the relevance of the breakup process in this energy range.

These strong channels clearly have an impact on the elastic scattering process and, in fact, large deviations from Rutherford scattering were observed even at deep sub-barrier energies for many systems—see, for instance, Refs. [28,31]—together with the disappearance of the Coulomb-nuclear interference peak. In this respect a measurement of the elastic scattering process, which for very low intensity Radioactive Ion Beams (RIBs) is sometimes the only feasible one, has a double utility:

- (1) It provides gross information concerning the reactivity of an exotic projectile via the extraction of the total reaction cross section.
- (2) It allows the investigation of the influence of nonelastic reaction channels (breakup, transfer, fusion, core excitations, etc.) on the elastic scattering angular distribution.

In this context we have performed the first measurement of the elastic scattering of the $1p$ -halo candidate ^8B from the heavy target ^{208}Pb at Coulomb barrier energies. ^8B is a very interesting nucleus: it is very weakly bound ($S_p = 137.5$ keV), it is the lightest particle stable boron isotope, and it plays a fundamental role in the production of high-energy neutrinos in the solar fusion model [32]. The reaction dynamics of this exotic projectile have already been investigated for a variety of targets, from ^{12}C to ^{58}Ni , in the energy range around the Coulomb barrier. The use of different targets helps exploration of the influence on the reaction dynamics of the different nuclear and Coulomb interactions and of transfer channels with different Q values. Before describing the experiment, we briefly summarize the main results of these studies.

Recently, Morcelle and coworkers measured the elastic scattering for the $^8\text{B} + ^{27}\text{Al}$ system at 15.3 and 21.7 MeV [33]. The experiment was partly performed at the Twinsol facility (University of Notre Dame, USA) [34] and partly at RIBRAS (São Paulo, Brazil) [35,36]. The authors noted that the breakup channel had a small, but not negligible, effect on the elastic scattering differential cross section and that it slightly damped the Coulomb rainbow peak originating from the interference between the nuclear and Coulomb interactions. As a result the ^8B reaction cross sections (in reduced units) were enhanced with respect to those for other light weakly bound projectiles interacting with a ^{27}Al target and were much larger than those for the doubly magic projectile ^{16}O .

Pakou and collaborators measured the α -particle production cross section for the $^8\text{B} + ^{28}\text{Si}$ system [37] and deduced the fusion cross section at four above-barrier energies via statistical model calculations. The experiment was performed at the EXOTIC facility (LNL, Italy) [38] by means of the active target technique. The trend of the experimental data was fairly well reproduced by the predictions of the Universal Fusion Function (UFF) [39].

By far the most studied system involving a ^8B projectile is $^8\text{B} + ^{58}\text{Ni}$, investigated in a series of experiments performed at TwinSol, beginning with the pioneering work of Guimarães and coworkers, who measured the ^7Be yield,

[§]Present address: School of Physics and Astronomy, University of Edinburgh, Peter Guthrie Tait Road, Edinburgh EH9 3FD, UK.

[†]Present address: Instituto de Física, Universidad Nacional Autónoma de México, Apartado Postal 20-364, Cd. Mx. 01000, Mexico.

[‡]Present address: Departamento de Física Atómica, Molecular y Nuclear, Universidad de Sevilla, Apartado 1065, E-41080 Sevilla, Spain.

[#]Deceased.

^{**}Present address: RIKEN, 2-1 Hirosawa, Wako, Saitama 351-0198, Japan.

essentially equivalent to the ${}^8\text{B} \rightarrow {}^7\text{Be} + p$ breakup cross section [40,41]. In the following years, Aguilera *et al.* [42] measured the elastic scattering at five energies around the Coulomb barrier. The extracted reaction cross section was as large as for the $2n$ -halo nucleus ${}^6\text{He}$ and turned out to be exhausted by the sum of the ${}^7\text{Be} + {}^{58}\text{Ni}$ total reaction cross section (measured in the same experiment) and the ${}^8\text{B}$ breakup cross section. Two years later the same group published a measurement of the fusion cross section for the same system at about ten near-barrier energies [43] and observed that the sum of the cross sections for the fusion and breakup processes exhausted the total reaction cross section. A simultaneous analysis, performed by Gomez-Camacho *et al.* [44], of the elastic scattering angular distributions and the fusion cross sections suggested that the so-called Breakup Threshold Anomaly (BTA) [45,46] occurred in this system. As the fusion data generated a controversy [47], the original data for the ${}^8\text{B} + {}^{28}\text{Si}$ and ${}^{58}\text{Ni}$ systems were critically reanalyzed [48] and the two fusion cross sections, when suitably reduced, were found to be in agreement within the error bars at the only overlapping energy point.

We may conclude that, for a ${}^8\text{B}$ projectile breakup, related effects tend to increase with the target mass as a consequence of the increasing predominance of the long-range Coulomb interaction with respect to the nuclear part of the potential. For this reason, we decided to investigate the elastic scattering process for the ${}^8\text{B} + {}^{208}\text{Pb}$ system at Coulomb barrier energies. The only existing measurements for this system, performed at Lanzhou (China), are at 170.3 [49] and 178 MeV [50], i.e., more than three times the Coulomb barrier. As expected for this bombarding energy [7], very small breakup effects on the elastic scattering differential cross section were observed. Our study was complemented by the first measurement of the elastic scattering process for the ${}^7\text{Be} + {}^{208}\text{Pb}$ system in the energy range around the Coulomb barrier, which was not only necessary to fix the core-target interaction in a ${}^7\text{Be} + p$ cluster model of ${}^8\text{B}$ but also of considerable interest in itself (see Ref. [51]), especially in relation to the similarities of ${}^7\text{Be}$ with the binding energy of ${}^6\text{Li}$ and the nuclear structure of ${}^7\text{Li}$, as underlined in the recent works by Sgouros and collaborators [52,53]. A quite comprehensive overview of previous experiments aimed at studying the ${}^7\text{Be}$ -induced reaction dynamics has been already given in Ref. [54].

The paper is organized as follows: Section II describes the ${}^8\text{B}$ and ${}^7\text{Be}$ RIB production and the detector setup used in the experiments. Section III illustrates the data reduction procedure required to obtain the elastic scattering angular distributions for both systems. The results of an optical model analysis are presented in Sec. IV and continuum discretized coupled channels (CDCC) calculations are described and compared with the data in Sec. V. The results are discussed in Sec. VI and some concluding remarks are made in Sec. VII.

II. EXPERIMENTS

A. ${}^8\text{B}$ secondary beam production

The ${}^8\text{B}$ RIB was produced by the in-flight technique with the CNS Radioactive Ion Beams (CRIB) facility [55] belonging to the Center for Nuclear Study (CNS) of the

University of Tokyo, located on the RIKEN campus at Wako (Saitama, Japan). A ${}^6\text{Li}^{3+}$ primary beam with an energy of 11.2 MeV/nucleon and an intensity of about $1\text{ p}\mu\text{A}$ was delivered by the AVF cyclotron and impinged on an 8-cm-long gas cell, doubly walled with 2.5- μm -thick Havar foils. The gas target was filled with ${}^3\text{He}$ gas at a pressure of 1 bar and kept at a cryogenic temperature ($\approx 90\text{ K}$) [56].

The ${}^8\text{B}$ beam was produced by means of the ${}^3\text{He}({}^6\text{Li}, {}^8\text{B})n$ two-body reaction ($Q = -1.97\text{ MeV}$). The secondary beam intensity on target was about 10^4 pps and the purity $\approx 20\%$, with ${}^7\text{Be}$, ${}^6\text{Li}$, and ${}^3\text{He}$ being the most intense contaminants. Before reaching the final focal plane the ${}^8\text{B}$ beam crossed two x - y sensitive Parallel Plate Avalanche Counters (PPACs) [57], located (for timing and beam reconstruction purposes) 669 and 439 mm upstream from the secondary target, and two collimators, displaced 306 mm (diameter 22 mm) and 180 mm (diameter 24 mm) upstream of the ${}^{208}\text{Pb}$ target. The ${}^8\text{B}$ beam energy on target was $50 \pm 1\text{ MeV}$.

B. ${}^8\text{B} + {}^{208}\text{Pb}$ experimental setup

Charged particles produced by the interaction between the ${}^8\text{B}$ secondary beam and a 2.2-mg/cm²-thick ${}^{208}\text{Pb}$ target (enrichment 99.57%) evaporated onto a 1.5- μm -thick mylar foil were detected by six modules of the EXPADES [58] detector array. Each module consisted of a double-sided silicon strip detector (DSSSD) ΔE - E_{res} telescope. The thicknesses of the ΔE and E_{res} stages were 43–57 and 300 μm , respectively. Each detector had an active area of 64.0 mm \times 64.0 mm and the front and rear sides were segmented into 32 strips in order to achieve a 2.0 mm \times 2.0 mm pixel resolution. However, to reduce the cost of the readout electronics, the strips of the ΔE layers were short circuited, two by two. Additional details on the detectors and the related electronics may be found in Ref. [58].

The EXPADES modules were located around the target position in a cylindrical configuration. The polar angle coverage of each telescope was $\theta_{\text{lab}} = [+8^\circ, +40^\circ]$ (telescope A), $[+50^\circ, +84^\circ]$ (B), $[-55^\circ, -85^\circ]$ (C), $[+95^\circ, +128^\circ]$ (D), $[-95^\circ, -125^\circ]$ (E), and $[-134^\circ, -166^\circ]$ (F). Positive and negative polar angles θ_{lab} refer to detectors displaced to the left and right, respectively, of the beam axis in a downstream view of the experimental setup. The central positions of the ΔE layers of telescopes A and F were located at a distance of 120 mm from the center of the target, while all other telescopes were at 110 mm. This configuration ensured a solid angle coverage of about 1.92 sr, corresponding to about 15% of 4π . The detectors were calibrated in energy in the range ≈ 3 –6 MeV by means of standard α calibration sources containing the following radioisotopes: ${}^{148}\text{Gd}$, ${}^{237}\text{Np}$, ${}^{241}\text{Am}$, and ${}^{244}\text{Cm}$. Typical energy resolutions were about 0.9% and 0.8% for ΔE and E_{res} layers, respectively.

The data acquisition system trigger condition employed was the AND of the anode signals of the two PPACs and the OR of the silicon detectors. Trigger rates of about 10–15 Hz were typically recorded during the experiment. The effective beam on target period was about 90 h. The energy loss in the rather thick ${}^{208}\text{Pb}$ target gives a mid-target beam energy of 49.35 MeV, within the uncertainty in the nominal beam energy

(50 ± 1 MeV), so a value of 50 MeV was used in the optical model and CDCC analyses.

C. ^7Be secondary beam production

The experiment with the ^7Be RIB was performed at the EXOTIC facility [38], installed at the Laboratori Nazionali di Legnaro (LNL) of the Istituto Nazionale di Fisica Nucleare (INFN), in Italy. The ^7Be beam was produced using the $^1\text{H}(^7\text{Li}, ^7\text{Be})n$ two-body reaction ($Q = -1.64$ MeV), following a procedure similar to that described in Ref. [54]. A $^7\text{Li}^{3+}$ primary beam, delivered by the LNL XTU-Tandem accelerator with an energy of 48.8 MeV and an intensity of 50–60 p nA, impinged on a gas target filled with H_2 gas. The gas cell was 5 cm long and the entrance and exit windows were made of 2.2- μm -thick Havar foils. In this experiment the beam also crossed two x - y sensitive PPACs (described in detail in Ref. [58]), located 900 and 365 mm upstream of the final focal plane of EXOTIC, before reaching the secondary target.

The first ^7Be energy of 40.5 ± 0.4 MeV was achieved by operating the target station at a gas pressure of 1 bar and at liquid nitrogen temperature (90 K). A second energy of 37.4 ± 0.5 MeV was obtained by inserting a 12.5- μm -thick aluminum degrader immediately behind the first PPAC. Finally, a third measurement at 42.2 ± 0.4 MeV was performed after warming up the target cell to room temperature and keeping the same hydrogen gas pressure inside. The secondary beam intensities were $(2\text{--}3) \times 10^5$ pps at the intermediate energy and about 10^5 pps and $(7\text{--}8) \times 10^4$ pps at the lowest and highest energies, respectively. The beam purity was about 99% at all energies.

D. $^7\text{Be} + ^{208}\text{Pb}$ experimental setup

The detector setup already described in Sec. II B was also used for the measurement of the charged particles produced by the interactions between the ^7Be projectiles and a self-supporting 1-mg/cm²-thick ^{208}Pb target (enrichment 99.57%). The six modules of EXPADES were also arranged in a cylindrical configuration around the target position in this experiment. The polar angle coverage of the telescopes was as follows: $\theta_{\text{lab}} = [+52^\circ, +85^\circ]$ (A), $[+95^\circ, +128^\circ]$ (B), $[+134^\circ, +171^\circ]$ (C), $[-52^\circ, -85^\circ]$ (D), $[-95^\circ, -128^\circ]$ (E), and $[-138^\circ, -167^\circ]$ (F). The central positions of the ΔE layers of detectors A–E were at an average distance of 111.5 mm from the center of the target. Telescope F was located a bit further away than the others at a distance of 141.5 mm. This arrangement guaranteed an overall solid angle coverage of 1.85 sr. The energy calibration was performed in the range $\approx 5\text{--}6$ MeV using triple sources with the following long-lived α emitters: ^{239}Pu , ^{241}Am , and ^{244}Cm . The energy resolutions were on average 1.1% for both ΔE and E_{res} telescope stages.

The trigger for the data acquisition system was provided by the AND condition between the cathode signals of both PPACs and the OR of the silicon detectors. Trigger rates of about 10 Hz were typical throughout the experiment. The acquisition times for data collection were about 24, 48, and 8 h for the lowest, intermediate and highest energies, respectively.

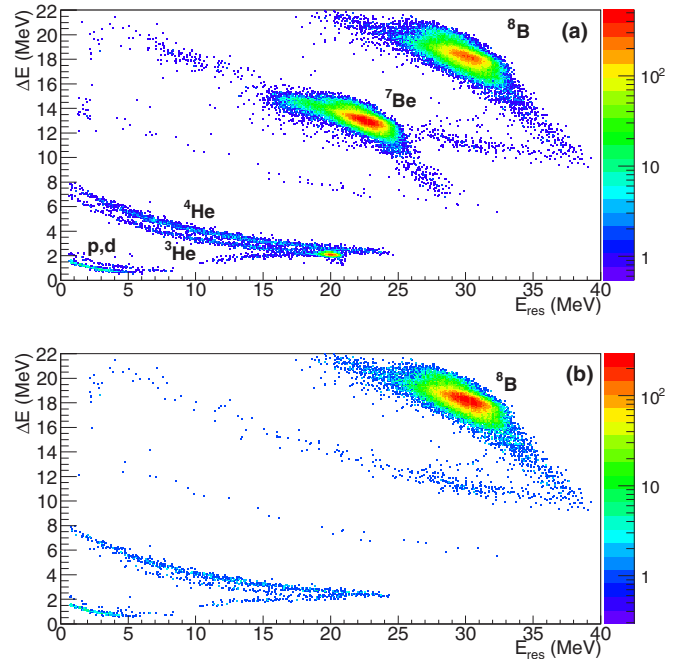


FIG. 1. (a) ΔE - E_{res} correlation plot for the $^8\text{B} + ^{208}\text{Pb}$ reaction at 50 MeV collected by telescope A, covering the polar angle range $\theta_{\text{lab}} = [+8^\circ, +40^\circ]$. The ^7Be and ^3He contaminant beams are clearly visible on the plot. (b) Same as (a) after imposing an RF gate on the incoming ^8B beam (see text for additional details).

We again used the nominal values for the beam energies in the optical model and CDCC analyses since the energy losses in the overall target thickness (≈ 400 keV) were within the uncertainties in the ^7Be secondary beam energies.

III. DATA ANALYSIS

A. $^8\text{B} + ^{208}\text{Pb}$ elastic scattering

The upper panels of Figs. 1 and 2 show two typical ΔE - E_{res} correlation plots collected by telescope A, located at forward angles, and telescope F, at backward angles, respectively. The events displayed correspond to those where only one detector strip on both the ΔE vertical and horizontal sides fired (with the two energy deposits within an uncertainty of ± 200 keV) and only one E_{res} horizontal strip. An energy threshold of approximately 250 keV was imposed on both telescope layers in the data reduction procedure, while charge sharing events, i.e., events releasing energy in the 40- μm -wide detector area in between two adjacent strips, were not considered in the present analysis. Due to gain instabilities it was not possible to use the energy information collected by the E_{res} vertical strips. The loci of the elastic scattering processes for the ^8B , ^7Be , and ^3He beams are clearly visible in Fig. 1(a) and are still distinguishable in Fig. 2(a) in spite of the much smaller statistics. In addition, the kinematic locations of other reaction products, such as ^4He , ^2H , and ^1H , can also be observed in both figures. As a remark, we observe that due to the excellent rejection capabilities of the CRIB facility only very few nuclei of the $1 \mu\text{A}$ ^6Li primary beam were able to reach the final focal plane.

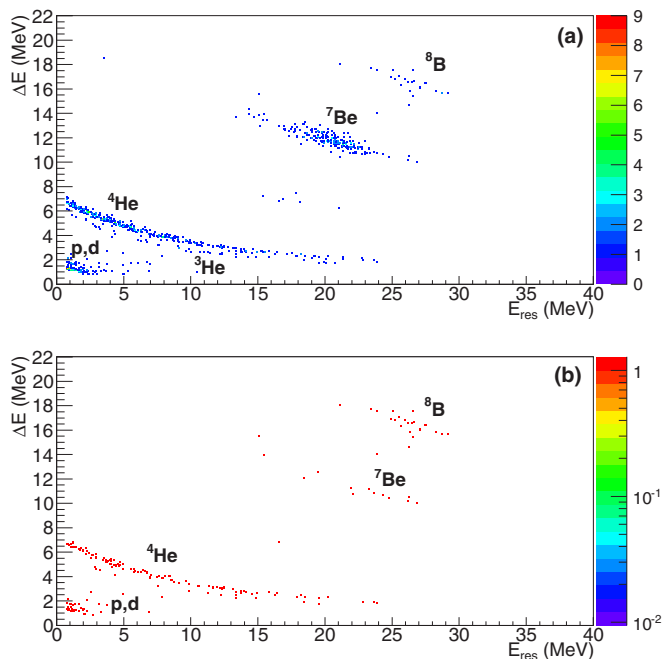


FIG. 2. As in Fig. 1, but for telescope F, located in the backward hemisphere ($\theta_{\text{lab}} = [-134^\circ, -166^\circ]$).

The lower panels of Figs. 1 and 2 show the same correlation plots as the upper panels after requiring a coincidence with the radio-frequency (RF) signal corresponding to the Time-of-Flight (ToF) of the ^8B secondary beam through CRIB. We can clearly see that the elastic peaks due to ^3He and ^7Be contaminant beams were suppressed to a large extent by this selection, while the remaining events should essentially originate from the interaction of the incoming ^8B beam with the ^{208}Pb target. The two-dimensional plot at backward angles [Fig. 2(b)] is rather clean and the surviving ^7Be should mainly originate from the $^8\text{B} \rightarrow ^7\text{Be} + p$ breakup channel, as we will discuss later.

Figure 3 presents the elastic scattering angular distribution for the $^8\text{B} + ^{208}\text{Pb}$ system at a beam energy of 50 MeV. To avoid the limited efficiency introduced by the shade of the mechanical support of the telescopes on the detector active areas, especially for marginal trajectories, events collected in the strips at the detector edges were not processed. Moreover, to compensate for statistical fluctuations, events from independent triggers gathered in adjacent ΔE vertical strips were grouped together and, where possible, the weighted averages of the differential cross sections computed by telescopes located at analogous polar angles in opposite hemispheres were employed. Of course, as can be seen in Fig. 3, this procedure is performed at the cost of a reduced angular resolution, especially at backward angles. We finally remark that the error bars displayed on Fig. 3 include the statistical uncertainty only.

In order to evaluate the elastic scattering differential cross section, we coded a Monte Carlo simulation following a procedure similar to those already employed in two previous experiments [54,59]. The code took into account the kinematics of the elastic scattering process, the Rutherford differential

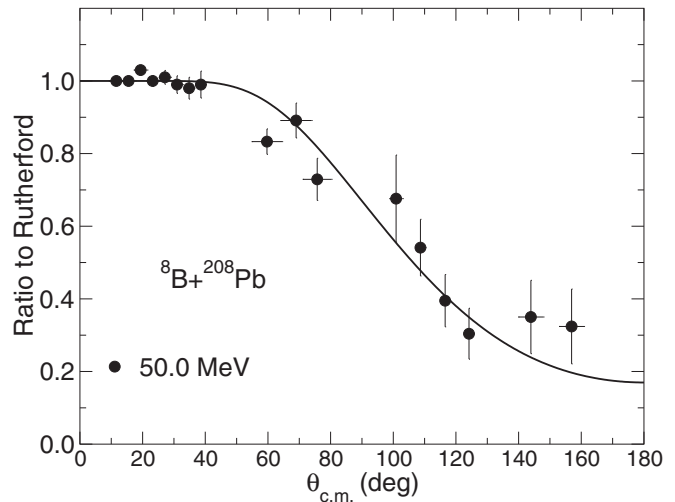


FIG. 3. Elastic scattering angular distribution for the $^8\text{B} + ^{208}\text{Pb}$ system at a beam energy of 50 MeV. Error bars are statistical only. The curve represents an optical model fit to the data; see text for more details.

cross section, the beam spot size on target and the beam divergence (reconstructed by means of the two PPACs), and the detector geometry. In the simulation a random interaction point within the target thickness was assumed and the energy loss prior to and after the scattering process was computed using a proper parameterization of the SRIM stopping power tables [60].

Theoretical calculations, described in detail in the following section, predicted an essentially pure (within the statistical accuracy of our measurement) Rutherford scattering process for polar angles smaller than 40° . Therefore, the experimental data were normalized, requiring the average value of the ratios to the Rutherford cross section evaluated for telescope A to be equal to unity. The systematic uncertainty introduced by the normalization procedure was estimated to be 2.5–3%. According to our analysis, no evidence for a Coulomb-nuclear interference peak appeared in the evaluation of the elastic scattering angular distribution, even if the value at $\theta_{\text{c.m.}} \approx 70^\circ$ clearly does not follow the trend described by the neighboring data points. This behavior is present in both individual evaluations obtained from telescopes B and C. After the rather steep decrease around 90° , the differential cross section tends to saturate to about one third of the Rutherford cross section for scattering angles larger than approximately 110° .

B. $^7\text{Be} + ^{208}\text{Pb}$ elastic scattering

Figure 4 displays three ΔE - E_{res} correlation plots for the $^7\text{Be} + ^{208}\text{Pb}$ reaction at 40.5 MeV for events collected by telescope A at forward angles (top panel), telescope B at backward angles (middle panel), and telescope F at very backward angles (bottom panel). In all plots the peaks related to the elastic scattering process are clearly visible, obviously with decreasing statistics as the scattering angle increases from forward to backward polar angles. The kinematic loci for isotopes of hydrogen, helium, and (at backward angles)

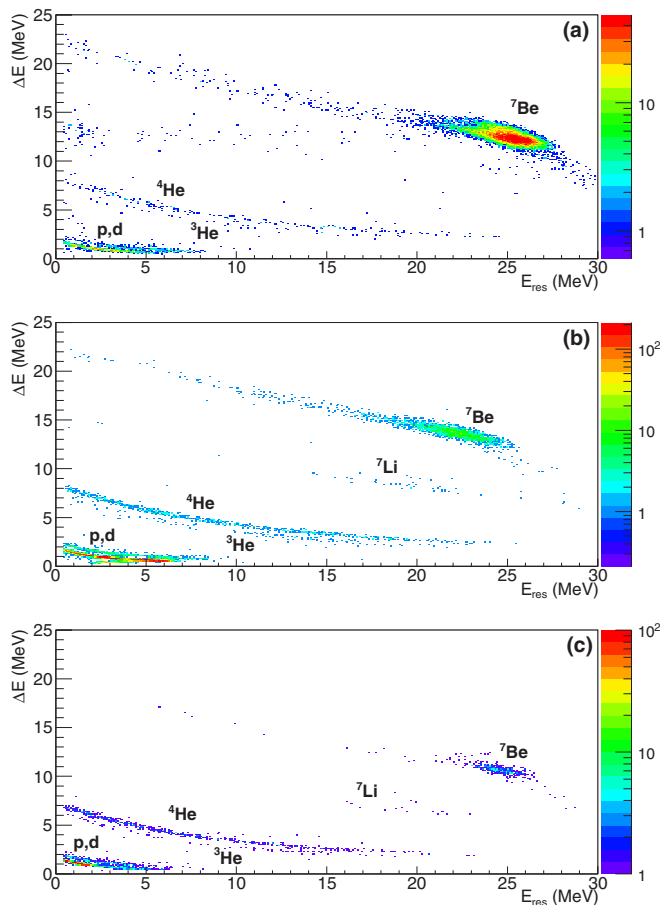


FIG. 4. ΔE - E_{res} correlation plots for the ${}^7\text{Be} + {}^{208}\text{Pb}$ reaction at 40.5 MeV registered by telescope A, $\theta_{\text{lab}} = [+52^\circ, +85^\circ]$ (a), telescope B, $\theta_{\text{lab}} = [+95^\circ, +128^\circ]$ (b), and telescope F, $\theta_{\text{lab}} = [-138^\circ, -167^\circ]$ (c). In addition to the elastic scattering peaks the kinematic loci related to the isotopes of hydrogen and helium produced by the interactions between the beam and the target are clearly visible.

lithium produced by the interactions between the ${}^7\text{Be}$ RIB and the ${}^{208}\text{Pb}$ target can also be distinguished in Fig. 4.

The data reduction followed a procedure very similar to that of the ${}^8\text{B} + {}^{208}\text{Pb}$ elastic scattering events. Again, we did not consider events registered in either the detector marginal strips or interstrip areas, and we selected only multiplicity-1 events for both ΔE vertical and horizontal strips and the E_{res} horizontal strips. Since the tandem accelerator provided a continuous primary beam no radio-frequency information was available for this experiment. However, since the secondary beam had a purity of 99%, the residual contamination had a negligible influence on the evaluation of the elastic scattering differential cross sections. To compensate for the large statistical fluctuations, events collected in adjacent ΔE vertical strips were grouped together. In this respect four differential cross section values per telescope were obtained for the data set at 40.5 MeV, whereas for the highest and lowest energies we employed only two multistrips, consisting of seven adjacent ΔE vertical strips, per telescope.

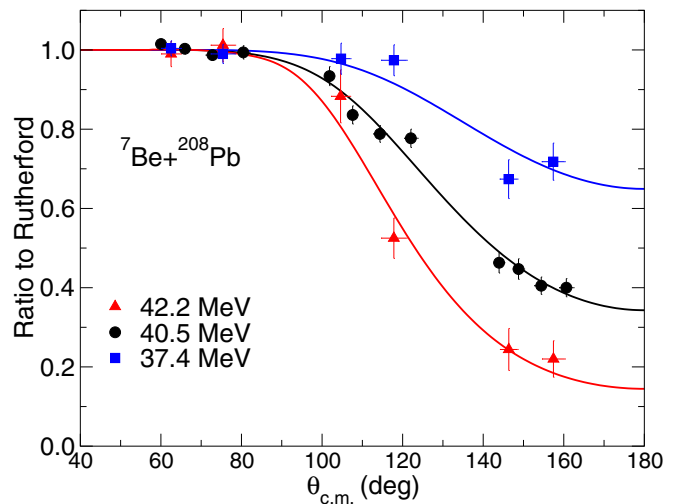


FIG. 5. Quasielastic differential cross section for ${}^7\text{Be} + {}^{208}\text{Pb}$ at beam energies of 42.2 MeV (red triangles), 40.5 MeV (black circles), and 37.4 MeV (blue squares). Errors bars are statistical only. The curves represent optical model fits to the data; see text for details.

Figure 5 presents the quasielastic scattering differential cross sections for the ${}^7\text{Be} + {}^{208}\text{Pb}$ reaction at 40.5 MeV (black circles), 37.4 MeV (blue squares), and 42.2 MeV (red triangles). Due to the secondary beam energy spread, target thickness, and detector energy resolution it was not possible to separate pure elastic scattering events from those leading to the excitation of the ${}^7\text{Be}$ first excited state at 0.429 MeV. Therefore, the data presented in Fig. 5 are “quasielastic,” consisting of the sum of these two processes. The errors plotted on Fig. 5 are statistical only.

As with the ${}^8\text{B}$ data, the normalization procedure was performed by means of a Monte Carlo simulation. We required that at all measured energies the differential cross sections for polar angles θ_{cm} smaller than 75 – 80° be equal (on average) to the Rutherford cross section since, according to theoretical calculations described later, pure Rutherford scattering was expected at these angles. The systematic uncertainty introduced by this procedure was estimated to be about 3% for the lowest and middle energies and up to 7% for the highest energy.

We also note that for the ${}^7\text{Be} + {}^{208}\text{Pb}$ reaction our data do not show any evidence of a Coulomb-nuclear interference peak before the sharp drop of the differential cross section due to the opening of nuclear reaction mechanisms. However, we emphasize that at the highest energy this peak, if present, would occur in the angular region where the target frame is positioned and therefore would not be covered by our detector setup.

IV. OPTICAL MODEL ANALYSIS

As a first step the data were analyzed using the optical model with volume Woods-Saxon potentials, principally to extract total reaction cross sections, σ_{R} . The data were fitted by χ^2 minimization using SFRESKO, the searching version of the FRESKO code [61].

TABLE I. Optical potential parameters obtained by fitting the ^8B and $^7\text{Be} + ^{208}\text{Pb}$ elastic scattering data. Total reaction cross sections (σ_R) are also reported. Radii follow the convention $R_i = r_i \times A_i^{1/3}$ fm and $r_C = 1.3$ fm.

Projectile	V	r_V	a_V	W	r_W	a_W	σ_R (mb)
^8B (50.0 MeV)	109.5	1.326	0.811	15.00	1.234	1.85	1112
^7Be (42.2 MeV)	134.3	1.326	0.811	14.42	1.534	0.884	371
^7Be (40.5 MeV)	128.1	1.326	0.811	15.71	1.534	0.884	253
^7Be (37.4 MeV)	194.8	1.326	0.811	19.05	1.534	0.884	121

The starting parameters for the 50 MeV $^8\text{B} + ^{208}\text{Pb}$ search were taken from the global ^6Li optical potential of Cook [62]. The resulting parameters are given in Table I, although, given the sparse nature of the data points and the relatively large uncertainties, the exact values have little physical significance beyond the observation of a definite preference for an imaginary potential with a large (>1.0) diffuseness parameter, a_W . The data were found to be relatively insensitive to the real part of the optical potential, therefore these parameters were held fixed at the values of the Cook global ^6Li potential and the parameters of the imaginary part only were varied. The resultant fit is shown by the solid curve on Fig. 3.

The $^7\text{Be} + ^{208}\text{Pb}$ quasielastic scattering data were fitted in a similar fashion. The slight error introduced into the fitting procedure by treating the data as pure elastic scattering was ignored since this was estimated to be within the statistical accuracy of the data. Test calculations found that the global ^6Li parameters of Cook [62] gave a better description of the ^7Be data than the ^7Li set, as predicted by the calculations presented in Ref. [51]. The ^6Li parameters were therefore used as a starting point for the fitting procedure. Again, given the sparse nature of the points and their limited statistics we did not attempt full parameter space searches. It was found that varying the real and imaginary well depths was sufficient to obtain good descriptions of the data at each energy. However, the exact values of these parameters are again without much physical significance, particularly at the lowest beam energy, mainly due to the sparseness of the data points.

Overall, we estimate the total reaction cross sections extracted in this way to have uncertainties of the order of 20%, typical for RIB data of this type.

V. CONTINUUM DISCRETIZED COUPLED CHANNELS CALCULATIONS

The data were further analyzed by means of CDCC calculations, explicitly taking into account the $^8\text{B} \rightarrow ^7\text{Be} + p$ and $^7\text{Be} \rightarrow ^4\text{He} + ^3\text{He}$ breakup processes. The calculations are fully described in the following two subsections. All calculations were carried out with the FRESKO code [61].

A. The $^8\text{B} + ^{208}\text{Pb}$ case

The CDCC calculations for the 50 MeV $^8\text{B} + ^{208}\text{Pb}$ data assumed a $^7\text{Be} + p$ cluster model of ^8B with an inert ^7Be core. The model was further simplified by setting the spin of the ^7Be core to zero, in order to avoid the prohibitive

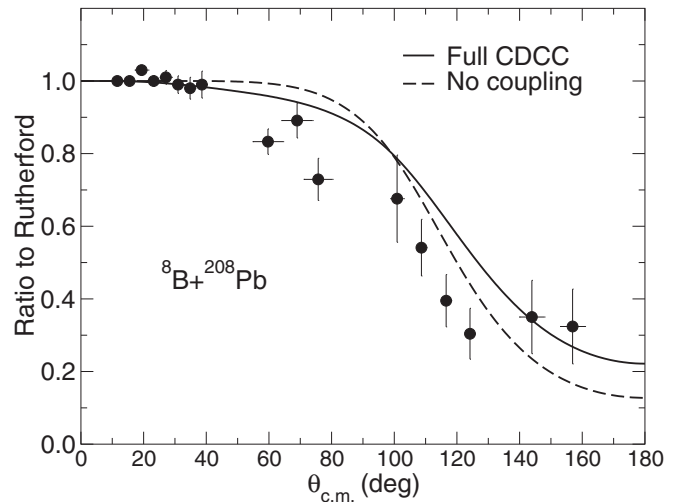


FIG. 6. Elastic scattering angular distribution for the $^8\text{B} + ^{208}\text{Pb}$ system at a beam energy of 50 MeV. The solid curve denotes the result of the full CDCC calculation while the dashed curve denotes that of the no-coupling case.

computational overhead of calculations including the full spin. Tests confirmed that the omission of the core spin made a negligible difference to the results. Diagonal and transition potentials were calculated using the cluster folding model [63]. The $^7\text{Be} + p$ binding potential was taken from Ref. [64] (including the spin-orbit term, since the proton spin was retained in our model) and the proton was considered to be in a pure $p_{3/2}$ state. The cluster folding model further requires optical model potentials for the core + target and cluster + target at the same incident energy per nucleon as the projectile, in this case 43.75 and 6.25 MeV for $^7\text{Be} + ^{208}\text{Pb}$ and $p + ^{208}\text{Pb}$, respectively. The $^7\text{Be} + ^{208}\text{Pb}$ optical potential employed the parameters of the fit to the 42.2 MeV data given in Table I and the $p + ^{208}\text{Pb}$ optical potential used the 9 MeV parameters from Table I of Ref. [65].

The $^7\text{Be} + p$ continuum was divided up into bins in momentum (k) space of width $\Delta k = 0.1 \text{ fm}^{-1}$ up to a maximum value $k_{\text{max}} = 0.7 \text{ fm}^{-1}$, corresponding to a maximum energy above the breakup threshold of 11.7 MeV. Angular momenta of the $^7\text{Be} + p$ relative motion $L = 0-5 \hbar$ were included in the binning scheme with couplings (including continuum-continuum couplings) up to multipolarity $\lambda = 5$. This continuum space was found to give adequate convergence of both the elastic scattering and the breakup cross sections.

The resulting elastic scattering angular distribution is compared with the data in Fig. 6, together with the no-coupling result. The total reaction cross section given by the full CDCC calculation is 1020 mb and the total $^8\text{B} \rightarrow ^7\text{Be} + p$ breakup cross section is 619 mb. Of this, approximately 46% is due to dipole breakup, where in order to estimate the dipole component we have assumed that the continuum bins with relative $p + ^7\text{Be}$ angular momenta $L = 0$ and 2 are solely populated by direct $\Delta L = 1$ excitation from the ground state (in reality there will also be some contribution from other ΔL 's via the continuum-continuum couplings, which we

assume to be small.) The no-coupling calculation yields a total reaction cross section of 558 mb.

Figure 6 shows that the breakup coupling effect, while not negligible, is hardly commensurate with the large breakup cross section. This is consistent with previous CDCC calculations for the interaction of ^8B with ^{208}Pb [4] and ^{58}Ni [4,66] targets. It is also apparent that the full calculation gives a relatively poor description of the elastic scattering data. A good description of the ^8B data can be obtained by multiplying the imaginary part of the cluster folding potential, including the transition potentials, by a factor of 2.5, possibly compensating for the influence of some effect missing from the simplified model of ^8B employed here. Since the similar CDCC calculations of Ref. [66] for the $^8\text{B} + ^{58}\text{Ni}$ system give a satisfactory description of the data (although there are hints of similar problems at some energies), this may be linked with the larger Coulomb field of the ^{208}Pb target.

B. The $^7\text{Be} + ^{208}\text{Pb}$ case

The $^7\text{Be} + ^{208}\text{Pb}$ CDCC calculations employed the $^3\text{He} + ^4\text{He}$ cluster model of ^7Be of Ref. [67]. In addition to the bound $1/2^-$ first excited state ($E_{\text{ex}} = 0.429$ MeV), the continuum space consisted of the two $L = 3\hbar$ resonances ($7/2^-$ and $5/2^-$ at $E_{\text{ex}} = 4.57$ and 6.73 MeV, respectively) plus the $L = 0-4\hbar$ nonresonant continuum. All couplings, including continuum-continuum couplings, up to a multipolarity of $\lambda = 4$ were included in the calculations. The continuum was divided into bins in k space of width $\Delta k = 0.1$ fm $^{-1}$ up to maximum values of $k_{\text{max}} = 0.9$ fm $^{-1}$, corresponding to a maximum energy above the breakup threshold of 9.88 MeV, for the calculations at beam energies of 42.2 and 40.5 MeV, and $k_{\text{max}} = 0.8$ fm $^{-1}$, corresponding to a maximum energy above the breakup threshold of 7.81 MeV, for the calculation at a beam energy of 37.4 MeV. This scheme was suitably modified in the presence of the two $L = 3\hbar$ resonances, which were treated as bins of width 0.4 and 2.0 MeV for the $7/2^-$ and $5/2^-$ states, respectively, to avoid double counting. This continuum space gave adequate convergence of both the elastic scattering and breakup cross sections.

The diagonal and transition potentials were again calculated using the cluster folding model. The $^3\text{He} + ^4\text{He}$ binding potential was taken from Ref. [67] and the $^4\text{He} + ^{208}\text{Pb}$ optical potentials were calculated using the global parameters of Ref. [68]. The $^3\text{He} + ^{208}\text{Pb}$ optical potentials for the 42.2 and 40.5 MeV calculations were obtained by refitting the 20 MeV $^3\text{He} + ^{208}\text{Pb}$ elastic scattering data of Ref. [69], yielding values of $V = 28.4$ MeV, $r_v = 1.50$ fm, $a_v = 0.60$ fm, $W = 9.17$ MeV, $r_w = 1.50$ fm, and $a_w = 0.60$ fm, with the form factors being of volume Woods-Saxon type and the radii given by $R_i = r_i \times 208^{1/3}$ fm. The Coulomb radius parameter was $r_C = 1.50$ fm. As the calculation at 37.4 MeV required a $^3\text{He} + ^{208}\text{Pb}$ optical potential for a ^3He energy of 16 MeV, significantly lower than 20 MeV, and no suitable data are available at this energy, the real and imaginary depths of the $^3\text{He} + ^{208}\text{Pb}$ optical potential were tuned to obtain the best description of the $^7\text{Be} + ^{208}\text{Pb}$ elastic scattering at this energy by the full CDCC calculation. This was achieved by multiplying both by a factor of 2.0.

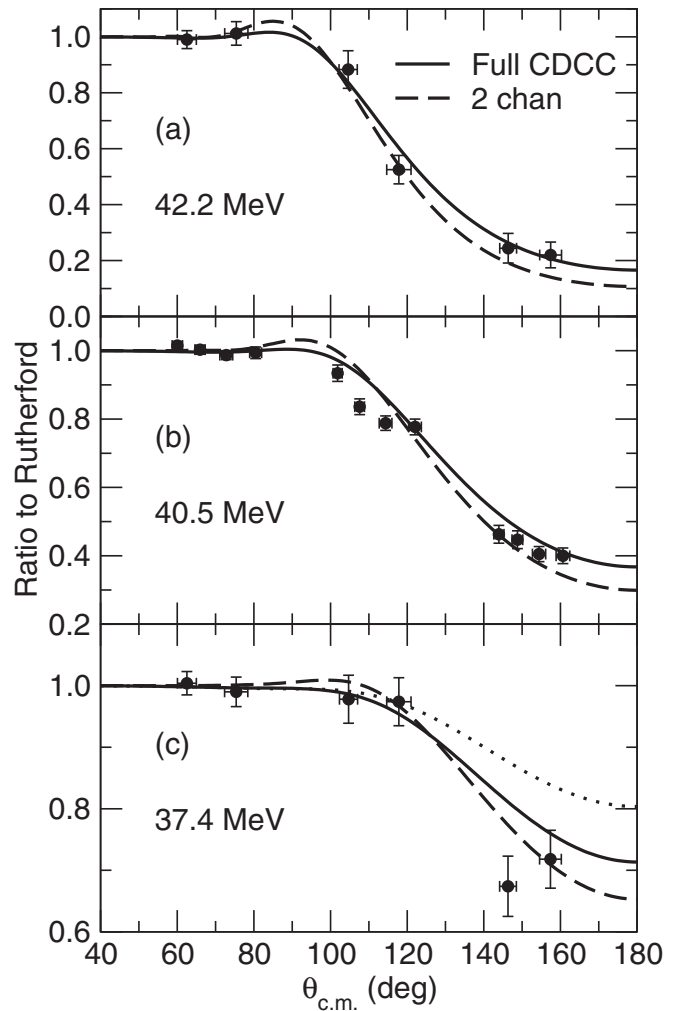


FIG. 7. Quasielastic scattering angular distributions for the $^7\text{Be} + ^{208}\text{Pb}$ system at beam energies of 42.2 (a), 40.5 (b), and 37.4 (c) MeV. The solid curves denote the results of the full CDCC calculation while the dashed curves denote those of the two-channel case; see text for details. The dotted curve at 37.4 MeV denotes the quasielastic scattering predicted by a full CDCC calculation using the same $^3\text{He} + ^{208}\text{Pb}$ optical model potential as at 42.2 and 40.5 MeV.

The resulting quasielastic scattering angular distributions are compared with the data in Fig. 7. Also shown on the figure are the quasielastic scattering angular distributions obtained from two-channel calculations including ground state reorientation and coupling to the bound $1/2^-$ state of ^7Be only. These results are shown in preference to the no-coupling cases since they represent the simplest coupling scheme that will yield a quasielastic scattering cross section.

The description of the data at 42.2 and 40.5 MeV by the CDCC calculations is good, especially when it is recalled that no tuning of parameters was involved at these energies. The description of the 37.4 MeV data is also good, although here the $^3\text{He} + ^{208}\text{Pb}$ optical potential was tuned to yield a better description. Tests with different ^3He and $^4\text{He} + ^{208}\text{Pb}$ optical potentials found that the choice of a realistic $^3\text{He} + ^{208}\text{Pb}$ potential, i.e., one that described scattering data at

TABLE II. Total reaction (σ_R) and breakup (σ_{bu}) cross sections for ${}^7\text{Be} + {}^{208}\text{Pb}$ obtained from the CDCC and two-channel calculations; see text for details.

Energy	Two-channel calculation	Full CDCC
42.2 MeV	$\sigma_R = 475$ mb	$\sigma_R = 463$ mb $\sigma_{\text{bu}} = 38$ mb
40.5 MeV	$\sigma_R = 339$ mb	$\sigma_R = 337$ mb $\sigma_{\text{bu}} = 30$ mb
37.4 MeV	$\sigma_R = 222$ mb	$\sigma_R = 225$ mb $\sigma_{\text{bu}} = 20$ mb

the appropriate energy (3/7 of the ${}^7\text{Be}$ beam energy) was essential to a good description of the 42.2 and 40.5 MeV data. The calculations were found to be relatively insensitive to the choice of ${}^4\text{He} + {}^{208}\text{Pb}$ potential. These findings provide the justification for tuning the ${}^3\text{He} + {}^{208}\text{Pb}$ potential for the calculation at 37.4 MeV. To further emphasize the need to tune the ${}^3\text{He} + {}^{208}\text{Pb}$ optical potential in order to obtain a good description of the 37.4 MeV data, we plot in Fig. 7(c) the quasielastic scattering from a full CDCC calculation at 37.4 MeV using the same ${}^3\text{He} + {}^{208}\text{Pb}$ optical potential as at 42.2 and 40.5 MeV. It significantly overpredicts the backward angle data points.

The total reaction cross sections for the two-channel and full CDCC calculations and the total ${}^7\text{Be} \rightarrow {}^4\text{He} + {}^3\text{He}$ breakup cross sections for the full CDCC calculations are given in Table II. Note that the breakup cross sections are a relatively small fraction of the total reaction cross section (of the order of 10%). Approximately 13% of the breakup is dipole at 42.2 MeV, increasing to about 34% at 40.5 and 37.4 MeV (the dipole contributions were estimated by summing the breakup cross sections for continuum bins where the ${}^3\text{He} + {}^4\text{He}$ relative angular momenta were $L = 0$ and 2, so will again contain some contribution from other ΔL values). The reduction in the total reaction cross section at 42.2 and 40.5 MeV caused by the addition of coupling to breakup is by no means unusual and has already been remarked on; see, e.g., Ref. [70].

VI. DISCUSSION

The optical model fits described in Sec. IV yield a much larger total reaction cross section for the ${}^8\text{B} + {}^{208}\text{Pb}$ system than for ${}^7\text{Be} + {}^{208}\text{Pb}$. This might be *a priori* expected due to the order-of-magnitude lower breakup threshold for ${}^8\text{B}$ (0.1375 MeV for the ${}^8\text{B} \rightarrow {}^7\text{Be} + p$ process) compared to that for ${}^7\text{Be}$ (1.5866 MeV for the ${}^7\text{Be} \rightarrow {}^4\text{He} + {}^3\text{He}$ process). The CDCC calculations of Sec. V appear to confirm this expectation since they predict a ${}^8\text{B}$ breakup cross section over an order of magnitude larger than those for ${}^7\text{Be}$. However, breakup is seldom the dominant direct contribution to the total reaction cross section for systems involving weakly bound projectiles, so it is of interest to compare these values with those obtained for similar systems.

In Fig. 8 we plot the total reaction cross sections for the ${}^8\text{B} + {}^{208}\text{Pb}$ and ${}^7\text{Be} + {}^{208}\text{Pb}$ systems derived from the

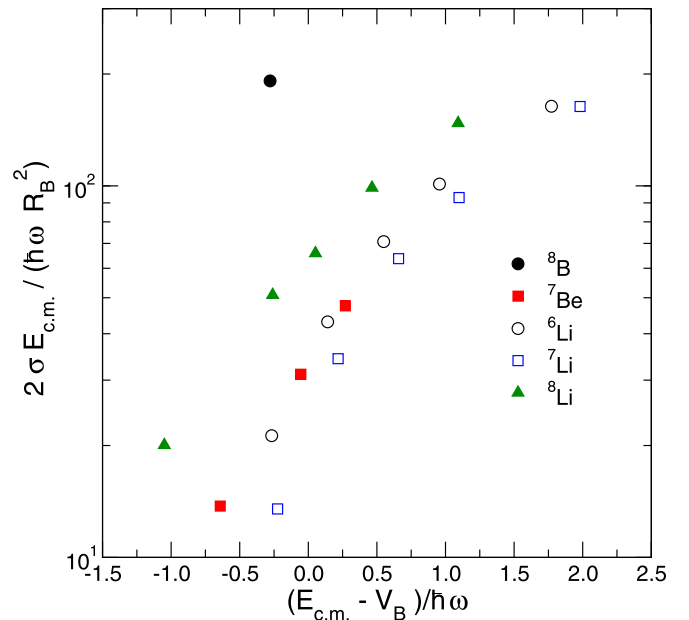


FIG. 8. Total reaction cross sections for the ${}^8\text{B}$, ${}^7\text{Be}$, ${}^6\text{Li}$, ${}^7\text{Li}$, and ${}^8\text{Li} + {}^{208}\text{Pb}$ systems extracted from optical model fits plotted on the dimensionless scale according to the formalism of Canto *et al.* [73].

present optical model fits with those for the ${}^{6,7}\text{Li} + {}^{208}\text{Pb}$ [71] and ${}^8\text{Li} + {}^{208}\text{Pb}$ [72] systems on the dimensionless scale according to the formalism of Canto *et al.* [73]. The Coulomb barrier radii, heights, and curvatures required for the reduction procedure were calculated using the São Paulo potential [74] and are given in Table III. The formalism of Canto *et al.* provides a convenient means of eliminating the gross effects of the different projectile charges and what might be termed the “geometrical” contribution to the total reaction cross section due to the different projectile radii. This method, originally developed for the comparison of the fusion cross sections, can still be meaningfully employed, even if with the severe limitations described in Ref. [75], for reaction cross section data, especially in this case where we are comparing projectiles with very similar masses and all interacting with the same target nucleus.

Figure 8 confirms the exceptionally large value of the total reaction cross section for ${}^8\text{B}$, as noted for the lighter ${}^{58}\text{Ni}$ target [42]. It also shows that, after the reduction procedure, the lowest total reaction cross sections are for the ${}^7\text{Li} + {}^{208}\text{Pb}$ system, with the ${}^6\text{Li} + {}^{208}\text{Pb}$ and ${}^7\text{Be} + {}^{208}\text{Pb}$ systems

TABLE III. Coulomb barrier radius R_B , height V_B , and curvature $\hbar\omega$ for the systems plotted in Fig. 8 calculated using the São Paulo potential [74].

System	R_B (fm)	V_B (MeV)	$\hbar\omega$ (MeV)
${}^8\text{B} + {}^{208}\text{Pb}$	11.16	49.40	4.49
${}^7\text{Be} + {}^{208}\text{Pb}$	11.19	39.45	5.09
${}^6\text{Li} + {}^{208}\text{Pb}$	11.25	29.46	4.77
${}^7\text{Li} + {}^{208}\text{Pb}$	11.43	29.04	4.39
${}^8\text{Li} + {}^{208}\text{Pb}$	11.59	28.68	4.08

having similar, slightly larger values, with the ${}^8\text{Li} + {}^{208}\text{Pb}$ total reaction cross sections intermediate between these latter and the ${}^8\text{B} + {}^{208}\text{Pb}$ value. The total reaction cross section is therefore not simply correlated with the breakup threshold for these light, weakly bound projectiles. This is explained by the fact that transfer processes provide the most important direct contribution to the total reaction cross section for these systems, with the exception of ${}^8\text{B} + {}^{208}\text{Pb}$, and the magnitude of transfer cross sections depends on a combination of factors including Q matching conditions rather than simply the Q value as such: spectroscopic factors, the availability of suitable levels in the targetlike residual nucleus, etc.

The CDCC calculations for ${}^8\text{B}$, which explicitly include coupling to the ${}^8\text{B} \rightarrow {}^7\text{Be} + p$ breakup, assume a simplified ${}^7\text{Be} + p$ cluster model of ${}^8\text{B}$ which treats the ${}^7\text{Be}$ core as inert, i.e., the possibility that the core itself may be excited is ignored. As noted previously, the description of the 50 MeV elastic scattering data by this model is relatively poor although a similar model gave a rather good description of near-barrier data for ${}^8\text{B} + {}^{58}\text{Ni}$ elastic scattering [66] and higher-energy (approximately three times the Coulomb barrier) ${}^8\text{B} + {}^{208}\text{Pb}$ elastic scattering [49]. This apparent discrepancy may be due to several reasons:

- (1) The choice of ${}^7\text{Be} + {}^{208}\text{Pb}$ and $p + {}^{208}\text{Pb}$ optical potential parameters used to calculate the cluster folded ${}^8\text{B} + {}^{208}\text{Pb}$ potential is significant.
- (2) Couplings to other reaction processes (essentially transfer reactions in this case) not included in the coupling scheme are important.
- (3) The model itself is too simplistic in this case in ignoring the possibility of core excitation.

Taking each point in turn, we first consider the question of the influence of the choice of ${}^7\text{Be} + {}^{208}\text{Pb}$ and $p + {}^{208}\text{Pb}$ optical potentials used as input to the ${}^8\text{B} + {}^{208}\text{Pb}$ cluster folding potential. For ${}^7\text{Be} + {}^{208}\text{Pb}$ the 42.2 MeV data presented in this work are at almost exactly the required energy so that the potential parameters may be fixed by fitting these data. There will of course be many parameter sets that give equivalent descriptions of the data; however, tests found that any physically reasonable set that fits these data gives a description of the ${}^8\text{B} + {}^{208}\text{Pb}$ data identical to that shown in Fig. 6 when used as input to the CDCC calculation. The influence of the $p + {}^{208}\text{Pb}$ optical potential is more difficult to evaluate since the required energy is below the relevant Coulomb barrier, and even if data existed they would be insensitive to the nuclear potential, because the elastic scattering is essentially pure Rutherford. However, tests were carried out using a variety of global parametrizations and potentials fitted to data at slightly higher energies and the final results presented in Fig. 6 correspond to the best description that was obtained, using the $p + {}^{208}\text{Pb}$ potential of Ref. [65].

Concerning the question of the influence of other reaction channel couplings, test calculations including the ${}^{208}\text{Pb}({}^8\text{B}, {}^7\text{Be}){}^{209}\text{Bi}$, ${}^{208}\text{Pb}({}^8\text{B}, {}^9\text{C}){}^{207}\text{Tl}$, and ${}^{208}\text{Pb}({}^8\text{B}, {}^9\text{B}){}^{207}\text{Pb}$ reactions were performed. In each case not only the cross sections but also the coupling effects on the elastic scattering were found to be negligible. The effect of coupling

to other reactions cannot be reliably quantified due to lack of suitable spectroscopic factors, for example, but the available evidence suggests that it is unlikely that missing couplings can account for the discrepancy between the CDCC calculations and the data.

Finally, there is the question as to whether the model of ${}^8\text{B}$ used in the CDCC calculations is too simplistic in ignoring the possibility of core excitation. At first sight this appears to be ruled out by the good description of the 170.3 MeV ${}^8\text{B} + {}^{208}\text{Pb}$ elastic scattering data [49] and the near-barrier ${}^8\text{B} + {}^{58}\text{Ni}$ data [66] by calculations employing a similar model. However, the data of Ref. [49] are well above the barrier (approximately three times the Coulomb barrier energy) where coupling effects are minimal, thus they do not constitute a rigorous check of the model. The calculations of Ref. [66] provide a good overall description of data at several near-barrier energies, although at some energies there are hints of problems similar to those found in this work. It is difficult to assess whether these are significant due the relatively large error bars in the ${}^8\text{B} + {}^{58}\text{Ni}$ data (due to the difficulty of producing a low-energy ${}^8\text{B}$ beam) but they are certainly smaller than in the present case. Taken together, these results suggest that the greater importance of the Coulomb field for the ${}^{208}\text{Pb}$ target at low energies may be instrumental in the relatively poor description of the present data. It is possible that it emphasizes the omission of core excitation in the ${}^8\text{B}$ model and that couplings to ground state reorientation, the bound $1/2^-$ first excited state, and, possibly, the two $L = 3$ resonances and/or the nonresonant continuum of the ${}^7\text{Be}$ core may play a significant role in the ${}^8\text{B}$ breakup process under these circumstances, or at least in its coupling effect on the elastic scattering. More data for the elastic scattering of ${}^8\text{B}$ from heavy targets at near-barrier energies will be required to confirm this, although Ref. [76] demonstrates that target charge does have an influence on the qualitative nature of the near-barrier ${}^8\text{B}$ elastic scattering angular distributions calculated using this model; the static effect first suggested in Ref. [43] in connection with fusion, and which manifests itself in the elastic scattering as a suppression of the Coulomb rainbow peak even in the no-coupling calculations, becomes more pronounced for heavier targets. Pseudo *et al.* [31] have shown conclusively that, for the somewhat analogous situation of the single-neutron halo nucleus ${}^{11}\text{Be}$ scattering from a ${}^{197}\text{Au}$ target at near-barrier energies, inclusion of the excitation of the ${}^{10}\text{Be}$ core to its 2_1^+ excited state was essential to a good simultaneous description of elastic and inelastic scattering and breakup. Thus it is certainly possible that core excitation could play a similar role in the case of ${}^8\text{B}$.

Figure 6 also shows that, despite the large calculated breakup cross section exhausting approximately 60% of the total reaction cross section, the coupling effect of breakup on the ${}^8\text{B}$ elastic scattering is modest. This is consistent with previous results, e.g., [4,66]. It remains unclear why this should be so, although it may also be linked with the fact that the ${}^7\text{Be}$ core nucleus is itself weakly bound.

The ${}^7\text{Be} + {}^{208}\text{Pb}$ data are well described by CDCC calculations using the two-body ${}^4\text{He} + {}^3\text{He}$ cluster model of Ref. [67]. The breakup couplings produce a significant reduction of the Coulomb rainbow peak compared to the

two-channel calculations that included couplings to ground state reorientation and excitation of the (bound) $1/2^-$ first excited state of ${}^7\text{Be}$ only. However, unfortunately the available data are unable to confirm this behavior, predicted in Ref. [51], since the experimental setup did not permit data collection at the necessary scattering angles.

The data do confirm the general validity of the model, particularly at 42.2 and 40.5 MeV where a good description was obtained with no tuning of inputs. Use of a ${}^3\text{He} + {}^{208}\text{Pb}$ optical potential in the cluster folding procedure that described the elastic scattering at the appropriate energy was crucial to this agreement. The lack of suitable data of this type was the main reason that the 34.7 MeV data required tuning of the ${}^3\text{He} + {}^{208}\text{Pb}$ potential parameters in order to obtain a reasonable description of the ${}^7\text{Be}$ quasielastic scattering data. It appears that in calculations of this type the quality of the description of the data is much more sensitive to the cluster + target optical potential than the core + target one. It would be worth following up this suggestion in other similar systems in order to test whether this is a universal phenomenon.

While the effect of coupling to the ${}^7\text{Be} \rightarrow {}^4\text{He} + {}^3\text{He}$ breakup on the ${}^7\text{Be} + {}^{208}\text{Pb}$ (quasi)elastic scattering angular distributions is similar to that of the ${}^8\text{B} \rightarrow {}^7\text{Be} + p$ breakup on the ${}^8\text{B} + {}^{208}\text{Pb}$ elastic scattering, the breakup cross section is much smaller (around 10% of the total reaction cross section for ${}^7\text{Be}$ compared to approximately 60% for ${}^8\text{B}$). This is a further example of the phenomenon of the coupling effect of a given reaction process on the elastic scattering not always being correlated with the cross section for that process. It also emphasizes the exceptional nature of the (predicted) breakup cross section for ${}^8\text{B}$. Dipole breakup is important for both systems, accounting for almost half of the total breakup cross section for ${}^8\text{B}$ and about one third of that for ${}^7\text{Be}$ at a similar “reduced” incident energy.

VII. SUMMARY AND CONCLUSIONS

New data were presented for the near-barrier elastic scattering of ${}^8\text{B}$ and ${}^7\text{Be}$ from ${}^{208}\text{Pb}$ (the ${}^7\text{Be}$ data being in fact quasielastic scattering since inelastic excitation of the 0.429 MeV $1/2^-$ state could not be resolved). The data were fitted using the optical model and total reaction cross sections extracted, with that for ${}^8\text{B}$ being much larger than for ${}^7\text{Be}$. CDCC calculations using a ${}^4\text{He} + {}^3\text{He}$ cluster model described the ${}^7\text{Be}$ data well, as expected since a similar model describes well the near-barrier elastic scattering of the mirror nucleus ${}^7\text{Li}$. The calculations confirm the predictions of Ref. [51] that the ${}^7\text{Be} + {}^{208}\text{Pb}$ elastic scattering angular distributions should be qualitatively more like those for ${}^6\text{Li} + {}^{208}\text{Pb}$ than ${}^7\text{Li} + {}^{208}\text{Pb}$, with a suppressed Coulomb rainbow peak, although the data cannot confirm this since the experimental setup did not allow the collection of data at the required scattering angles. However, the total reaction cross sections, when reduced according to the formalism of Canto *et al.* [73], do support the prediction of Ref. [51] that ${}^7\text{Be}$ should behave more like ${}^6\text{Li}$ than its mirror ${}^7\text{Li}$ when interacting with a ${}^{208}\text{Pb}$ target, since they match the ${}^6\text{Li}$ values rather than those for ${}^7\text{Li}$.

In contrast, the ${}^8\text{B} + {}^{208}\text{Pb}$ elastic scattering data were rather poorly described by CDCC calculations employing a simplified ${}^7\text{Be} + p$ cluster model where the ${}^7\text{Be}$ core was treated as inert. A similar model was able to describe well data for the same system at an incident energy of 170.3 MeV (approximately three times the Coulomb barrier) [49] and at near-barrier energies for the ${}^8\text{B} + {}^{58}\text{Ni}$ system [66]. It was suggested that the apparent discrepancy could be linked to the greater importance of the Coulomb interaction for the present data and may point to the need to include the possibility of core excitation in the model of ${}^8\text{B}$. Thus ${}^8\text{B}$ may be similar in this respect to the single-neutron halo nucleus ${}^{11}\text{Be}$ [31].

Our conclusions are as follows: ${}^7\text{Be}$ appears to behave exactly as expected and its (quasi)elastic scattering angular distributions seem well understood in the context of CDCC calculations using a ${}^4\text{He} + {}^3\text{He}$ cluster model, in agreement with what was found for the ${}^7\text{Be} + {}^{28}\text{Si}$ [53] and ${}^{58}\text{Ni}$ [54] systems. While the predicted suppression of the Coulomb rainbow peak for heavier targets remains to be confirmed experimentally, the good agreement obtained between the CDCC calculations and the measurements for three widely separated targets strongly supports the validity of the model. Use of a ${}^3\text{He} + {}^{208}\text{Pb}$ optical model potential that describes well the appropriate elastic scattering data as input to the cluster folding model was found to be essential to obtaining a good description of the ${}^7\text{Be}$ quasielastic scattering by the CDCC calculations. It would be interesting to investigate whether this is a universal phenomenon in studies of this type.

The relatively poor description of the ${}^8\text{B} + {}^{208}\text{Pb}$ elastic scattering data is most probably due to the increased importance of the Coulomb interaction emphasizing the omission of core excitation in the model of ${}^8\text{B}$ used. A good fit could be obtained by multiplying the imaginary well depth of the cluster folded ${}^8\text{B} + {}^{208}\text{Pb}$ potential by a factor of 2.5, suggesting that the influence of some effect missing from the model is being compensated. If it is indeed the omission of the core excitation that lies at the root of the problem, since the ${}^7\text{Be}$ core is itself weakly bound, it may be necessary to include excitation of its two $L = 3$ resonant states and/or the low-lying nonresonant continuum in the model, a formidable task that is beyond current formulations of CDCC. Further data for the elastic scattering of ${}^8\text{B}$ from heavy targets at near-barrier energies are desirable to confirm the apparent need to go further than the inert-core picture.

The final conclusion may be summed up very simply: while ${}^7\text{Be}$ appears to be well understood, ${}^8\text{B}$ remains something of an enigma [77].

ACKNOWLEDGMENTS

The ${}^8\text{B}$ experiment was performed at the RI Beam Factory operated by RIKEN Nishina Center and CNS, University of Tokyo. This work was supported by the Polish National Science Centre under Contract No. 2014/14/M/ST2/00738 (COPIN-INFN Collaboration), by JSPS KAKENHI (Grants No. 16K05369 and No. 19K03883) from the Ministry of Education, Culture, Sports, Science and Technology (MEXT) of Japan and by the projects CONACyT LN-294537 and DGAPA-PAPIIT IA103218.

- [1] L. F. Canto, P. R. S. Gomes, R. Donangelo, and M. S. Hussein, *Phys. Rep.* **424**, 1 (2006).
- [2] J. F. Liang and C. Signorini, *Int. J. Mod. Phys. E* **14**, 1121 (2005).
- [3] N. Keeley, R. Raabe, N. Alamanos, and J.-L. Sida, *Prog. Part. Nucl. Phys.* **59**, 579 (2007).
- [4] N. Keeley, N. Alamanos, K. W. Kemper, and K. Rusek, *Prog. Part. Nucl. Phys.* **63**, 396 (2009).
- [5] M. Mazzocco, *Int. J. Mod. Phys. E* **19**, 977 (2010).
- [6] B. B. Back, H. Esbensen, C. L. Jiang, and K. E. Rehm, *Rev. Mod. Phys.* **86**, 317 (2014).
- [7] N. Keeley, K. W. Kemper, and K. Rusek, *Eur. Phys. J. A* **50**, 145 (2014).
- [8] L. F. Canto, P. R. S. Gomes, R. Donangelo, J. Lubian, and M. S. Hussein, *Phys. Rep.* **596**, 1 (2015).
- [9] J. J. Kolata, V. Guimarães, and E. F. Aguilera, *Eur. Phys. J. A* **52**, 123 (2016).
- [10] A. S. Fomichev *et al.*, *Z. Phys. A* **351**, 129 (1995).
- [11] M. Trotta, J. L. Sida, N. Alamanos, A. Andreyev, F. Auger, D. L. Balabanski, C. Borcea, N. Coulier, A. Drouart, D. J. C. Durand *et al.*, *Phys. Rev. Lett.* **84**, 2342 (2000).
- [12] A. Di Pietro, P. Figuera, F. Amorini, C. Angulo, G. Cardella, S. Cherubini, T. Davinson, D. Leanza, J. Lu, H. Mahmud *et al.*, *Phys. Rev. C* **69**, 044613 (2004).
- [13] A. Navin, V. Tripathi, Y. Blumenfeld, V. Nanal, C. Simenel, J. M. Casandjian, G. de France, R. Raabe, D. Bazin, A. Chatterjee *et al.*, *Phys. Rev. C* **70**, 044601 (2004).
- [14] A. Chatterjee, A. Navin, A. Shrivastava, S. Bhattacharyya, M. Rejmund, N. Keeley, V. Nanal, J. Nyberg, R. G. Pillay, K. Ramachandran *et al.*, *Phys. Rev. Lett.* **101**, 032701 (2008).
- [15] D. Escrig *et al.*, *Nucl. Phys. A* **792**, 2 (2007).
- [16] A. M. Sánchez-Benítez *et al.*, *Nucl. Phys. A* **803**, 30 (2008).
- [17] L. Acosta, A. M. Sanchez-Benitez, M. E. Gomez, I. Martel, F. Perez-Bernal, F. Pizarro, J. Rodriguez-Quintero, K. Rusek, M. A. G. Alvarez, M. V. Andres *et al.*, *Phys. Rev. C* **84**, 044604 (2011).
- [18] J. P. Bychowski *et al.*, *Phys. Lett. B* **596**, 26 (2004).
- [19] P. A. De Young, P. J. Mears, J. J. Kolata, E. F. Aguilera, F. D. Becchetti, Y. Chen, M. Cloughesy, H. Griffin, C. Guess, J. D. Hinnfeld *et al.*, *Phys. Rev. C* **71**, 051601(R) (2005).
- [20] J. J. Kolata, H. Amro, F. D. Becchetti, J. A. Brown, P. A. De Young, M. Hencheck, J. D. Hinnfeld, G. F. Peaslee, A. L. Fritsch, C. Hall, U. Khadka, P. J. Mears, P. O' Rourke, D. Padilla, J. Rieth, T. Spencer, and T. Williams, *Phys. Rev. C* **75**, 031302(R) (2007).
- [21] R. Raabe *et al.*, *Nature (London)* **431**, 823 (2004).
- [22] A. Lemasson *et al.*, *Phys. Rev. Lett.* **103**, 232701 (2009).
- [23] A. Lemasson, A. Navin, N. Keeley, M. Rejmund, S. Bhattacharyya, A. Shrivastava, D. Bazin, D. Beaumel, Y. Blumenfeld, A. Chatterjee *et al.*, *Phys. Rev. C* **82**, 044617 (2010).
- [24] G. Marquín-Durán, I. Martel, A. M. Sanchez-Benitez, L. Acosta, R. Berjillos, J. Duenas, K. Rusek, N. Keeley, M. A. G. Alvarez, M. J. G. Borge *et al.*, *Phys. Rev. C* **94**, 064618 (2016).
- [25] G. Marquín-Durán, I. Martel, A. M. Sanchez-Benitez, L. Acosta, J. L. Aguado, R. Berjillos, A. R. Pinto, T. Garcia, J. A. Duenas, K. Rusek *et al.*, *Phys. Rev. C* **98**, 034615 (2018).
- [26] A. Pakou *et al.*, *Eur. Phys. J. A* **51**, 55 (2015).
- [27] K. J. Cook *et al.*, *Phys. Rev. C* **97**, 021601(R) (2018).
- [28] M. Cubero, J. P. Fernandez-Garcia, M. Rodriguez-Gallardo, L. Acosta, M. Alcorta, M. A. G. Alvarez, M. J. G. Borge, L. Buchmann, C. A. Diget, H. A. Falou *et al.*, *Phys. Rev. Lett.* **109**, 262701 (2012).
- [29] J. P. Fernandez-Garcia, M. Cubero, M. Rodriguez-Gallardo, L. Acosta, M. Alcorta, M. A. G. Alvarez, M. J. G. Borge, L. Buchmann, C. A. Diget, H. A. Falou *et al.*, *Phys. Rev. Lett.* **110**, 142701 (2013).
- [30] A. Di Pietro, G. Randisi, V. Scuderi, L. Acosta, F. Amorini, M. J. G. Borge, P. Figuera, M. Fisichella, L. M. Fraile, J. Gomez-Camacho *et al.*, *Phys. Rev. Lett.* **105**, 022701 (2010).
- [31] V. Pesudo, M. J. G. Borge, A. M. Moro, J. A. Lay, E. Nácher, J. Gómez-Camacho, O. Tengblad, L. Acosta, M. Alcorta, M. A. G. Alvarez *et al.*, *Phys. Rev. Lett.* **118**, 152502 (2017).
- [32] E. G. Adelberger, A. Garcia, R. G. Hamish Robertson, K. A. Snover, A. B. Balantekin, K. Heeger, M. J. Ramsey-Musolf, D. Bemmerer, A. Junghans, C. A. Bertulani *et al.*, *Rev. Mod. Phys.* **83**, 195 (2011).
- [33] V. Morcelle *et al.*, *Phys. Rev. C* **95**, 014615 (2017).
- [34] F. D. Becchetti *et al.*, *Nucl. Instrum. Methods Phys. Res., Sect. A* **505**, 377 (2003).
- [35] R. Lichtenthäler *et al.*, *Eur. Phys. J. A* **25**, 733 (2005).
- [36] A. Lepine-Szily, R. Lichtenthäler, and V. Guimarães, *Eur. Phys. J. A* **50**, 128 (2014).
- [37] A. Pakou, E. Stiliaris, D. Pierroutsakou, N. Alamanos, A. Boiano, C. Boiano, D. Filipescu, T. Glodariu, J. Grebosz, A. Guglielmetti *et al.*, *Phys. Rev. C* **87**, 014619 (2013).
- [38] F. Farinon *et al.*, *Nucl. Instrum. Methods Phys. Res., Sect. B* **266**, 4097 (2008).
- [39] L. F. Canto, P. R. S. Gomes, J. Lubian, L. C. Chamon, and E. Crema, *Nucl. Phys. A* **821**, 51 (2009).
- [40] V. Guimarães *et al.*, *Phys. Rev. Lett.* **84**, 1862 (2000).
- [41] J. J. Kolata *et al.*, *Phys. Rev. C* **63**, 024616 (2001).
- [42] E. F. Aguilera, E. Martínez-Quiroz, D. Lizcano, A. Gomez-Camacho, J. J. Kolata, L. O. Lamm, V. Guimaraes, R. Lichtenthäler, O. Camargo, F. D. Becchetti *et al.*, *Phys. Rev. C* **79**, 021601(R) (2009).
- [43] E. F. Aguilera, P. Amador-Valenzuela, E. Martínez-Quiroz, D. Lizcano, P. Rosales, H. Garcia-Martinez, A. Gomez-Camacho, J. J. Kolata, A. Roberts, L. O. Lamm *et al.*, *Phys. Rev. Lett.* **107**, 092701 (2011).
- [44] A. Gomez Camacho, E. F. Aguilera, P. R. S. Gomes, and J. Lubian, *Phys. Rev. C* **84**, 034615 (2011).
- [45] P. R. S. Gomes *et al.*, *J. Phys. G* **31**, S1669 (2005).
- [46] M. S. Hussein, P. R. S. Gomes, J. Lubian, and L. C. Chamon, *Phys. Rev. C* **73**, 044610 (2006).
- [47] J. Rangel *et al.*, *Eur. Phys. J. A* **49**, 57 (2013).
- [48] E. F. Aguilera, P. Amador-Valenzuela, E. Martínez-Quiroz, J. Fernandez-Arnaiz, J. J. Kolata, and V. Guimaraes, *Phys. Rev. C* **93**, 034613 (2016).
- [49] Y. Y. Yang *et al.*, *Phys. Rev. C* **87**, 044613 (2013).
- [50] Y. Y. Yang, X. Liu, D. Y. Pang, D. Patel, R. F. Chen, J. S. Wang, P. Ma, J. B. Ma, S. L. Jin, Z. Bai *et al.*, *Phys. Rev. C* **98**, 044608 (2018).
- [51] N. Keeley, K. W. Kemper, and K. Rusek, *Phys. Rev. C* **66**, 044605 (2002).
- [52] O. Sgouros, A. Pakou, D. Pierroutsakou, M. Mazzocco, L. Acosta, X. Aslanoglou, C. Betsou, A. Boiano, C. Boiano, D. Carbone *et al.*, *Phys. Rev. C* **94**, 044623 (2016).

- [53] O. Sgouros, A. Pakou, D. Pierroutsakou, M. Mazzocco, L. Acosta, X. Aslanoglou, Ch. Betsou, A. Boiano, C. Boiano, D. Carbone *et al.*, *Phys. Rev. C* **95**, 054609 (2017).
- [54] M. Mazzocco, D. Torresi, D. Pierroutsakou, N. Keeley, L. Acosta, A. Boiano, C. Boiano, T. Glodariu, A. Guglielmetti, M. La Commara *et al.*, *Phys. Rev. C* **92**, 024615 (2015).
- [55] Y. Yanagisawa *et al.*, *Nucl. Instrum. Methods Phys. Res., Sect. A* **539**, 74 (2005).
- [56] H. Yamaguchi *et al.*, *Nucl. Instrum. Methods Phys. Res., Sect. A* **589**, 150 (2008).
- [57] H. Kumagai, A. Ozawa, N. Fukuda, N. Sümmerer, and I. Tanihata, *Nucl. Instrum. Methods Phys. Res., Sect. A* **470**, 562 (2001).
- [58] D. Pierroutsakou *et al.*, *Nucl. Instrum. Methods Phys. Res., Sect. A* **834**, 46 (2016).
- [59] M. Mazzocco, C. Signorini, D. Pierroutsakou, T. Glodariu, A. Boiano, C. Boiano, F. Farinon, P. Figuera, D. Filipescu, L. Fortunato *et al.*, *Phys. Rev. C* **82**, 054604 (2010).
- [60] J. F. Ziegler, M. D. Ziegler, and J. P. Biersack, *Nucl. Instrum. Methods Phys. Res., Sect. B* **268**, 1818 (2010).
- [61] I. J. Thompson, *Comput. Phys. Rep.* **7**, 167 (1988).
- [62] J. Cook, *Nucl. Phys. A* **388**, 153 (1982).
- [63] B. Buck and A. A. Pilt, *Nucl. Phys. A* **280**, 133 (1977).
- [64] P. Navrátil, C. A. Bertulani, and E. Caurier, *Phys. Lett. B* **634**, 191 (2006).
- [65] R. W. Finlay, J. Wierzbicki, R. K. Das, and F. S. Dietrich, *Phys. Rev. C* **39**, 804 (1989).
- [66] J. Lubian, T. Correa, E. F. Aguilera, L. F. Canto, A. Gomez-Camacho, E. M. Quiroz, and P. R. S. Gomes, *Phys. Rev. C* **79**, 064605 (2009).
- [67] B. Buck and A. C. Merchant, *J. Phys. G* **14**, L211 (1988).
- [68] V. Avrigeanu, M. Avrigeanu, and C. Mănăilescu, *Phys. Rev. C* **90**, 044612 (2014).
- [69] R. W. Klingensmith, H. J. Hausman, and W. D. Ploughe, *Phys. Rev.* **134**, B1220 (1964).
- [70] R. S. Mackintosh, *Phys. Rev. C* **88**, 054603 (2013).
- [71] N. Keeley, S. J. Bennett, N. M. Clarke, B. R. Fulton, G. Tungate, P. V. Drumm, M. A. Nagarajan, and J. S. Lilley, *Nucl. Phys. A* **571**, 326 (1994).
- [72] J. J. Kolata, V. Z. Goldberg, L. O. Lamm, M. G. Marino, C. J. O’Keeffe, G. Rogachev, E. F. Aguilera, H. García-Martínez, E. Martínez-Quiroz, P. Rosales, F. D. Becchetti, T. W. O’Donnell, D. A. Roberts, J. A. Brown, P. A. DeYoung, J. D. Hinnefeld, and S. A. Shaheen, *Phys. Rev. C* **65**, 054616 (2002).
- [73] L. F. Canto, P. R. S. Gomes, J. Lubian, L. C. Chamon, and E. Crema, *J. Phys. G* **36**, 015109 (2009).
- [74] L. C. Chamon, B. V. Carlson, L. R. Gasques, D. Pereira, C. De Conti, M. A. G. Alvarez, M. S. Hussein, M. A. Cândido Ribeiro, E. S. Rossi, Jr., and C. P. Silva, *Phys. Rev. C* **66**, 014610 (2002).
- [75] L. F. Canto, D. R. Mendes, Jr., P. R. S. Gomes, and J. Lubian, *Phys. Rev. C* **92**, 014626 (2015).
- [76] Y. Kucuk and E. Aciksoz, *Eur. Phys. J. A* **52**, 98 (2016).
- [77] N. Keeley, *J. Phys.: Conf. Ser.* **381**, 012087 (2012).